Improved SHSAW Transduction Efficiency Using Grating and Uniform Electrode Guiding

Thomas B. Pollard, *Student Member, IEEE*, and Mauricio Pereira da Cunha, *Senior Member, IEEE*

***Abstract*—Pure shear-horizontal surface acoustic wave (SHSAW) devices have been increasingly considered for liquid-phase and biosensing applications because of their ability to operate under liquid-loaded conditions and intrinsic sensitivity to mass, stiffness, viscosity, and electrical perturbations occurring at the device/fluid interface. Typically, the SHSAW is weakly guided by a free surface boundary condition (BC) or may not even exist for some materials and orientations, such as the quartz ST-90° orientation considered in this work. For a surrounding free surface BC, the interdigital transducer (IDT) typically generates strong shear-horizontal bulk acoustic waves (SHBAWs) relative to SHSAW. For that reason, guiding structures, e.g., dense and/or thick electrodes in periodic or uniform configurations, are incorporated into the design and placed between IDTs in delay-line devices to increase the ratio of transduced SHSAW power to IDT input power, η_{SHSAW}. The degree of η_{SHSAW} improvement depends on the thickness, composition, and geometry of the guiding structure. In previous work, the authors evaluated η_{SHSAW} using hybrid finite and boundary element method (FEM/BEM) models, but were limited to cases of stress-free or finite-thickness-grating surrounding surfaces. This work extends the analysis to the important boundary condition case of uniform finite-thickness electrode guiding, which is typically employed in liquid-phase and biosensor applications. To integrate the uniform electrode guiding structure with the SHSAW device analysis, a combined finite-length uniform electrode structure followed by an additional quarter-wavelength electrode was considered. In this work, it is shown that adjusting the quarter-wavelength electrode's film thickness and length allows cancellation of the SHSAW reflection from the edge discontinuity. As a result, the finite-length uniform guiding electrode can be treated as if it extends to infinity, and η_{SHSAW} can be easily obtained. In addition, the finite thickness of all electrodes is considered in the calculations. To verify the model, an IDT with uniform guiding electrodes was simulated and compared with the experimental results of a fabricated and tested device. The simulations predict SHSAW excitation directivity of 9 dB by the IDT, which is experimentally confirmed to within 0.8 dB.**

I. Introduction

Biosensor and liquid-phase platform devices based on SAW technology typically require propagation under a liquid-loaded surface condition to probe the analyte of interest [1]–[3]. To satisfy this requirement, one may typically employ platform devices fabricated along crystallographic orientations which support SAW modes with strong transverse particle polarization, such as the pure shear-horizontal surface acoustic wave (SHSAW) mode; certain pseudo-SAW (PSAW) modes, e.g., 36° Y-rotated $LiTaO_3$; the Love mode; and the acoustic plate mode (APM) [3]–[6]. The use of modes with strong transverse particle polarization present reduced propagation losses compared with orientations supporting the general or Rayleigh-type SAW modes, because the latter excite a compression-type mode in the adjacent liquid media, normally resulting in severe mode dampening [3], [4], [7].

The pure piezoelectrically active SHSAW can exist along crystal orientations for which the electrical fields and the shear-horizontal mechanical displacement component uncouple from the purely mechanical sagittal displacement components, leading to two separate SAW solutions [8]: a stiffened shear-horizontal wave, the pure SHSAW; and a purely mechanical sagittal SAW (also referred to as purely mechanical Rayleigh SAW, with no particle displacement in the direction normal to the sagittal plane). This type of propagation direction has been classified as symmetry type 4 in [8]. Examples of crystals and orientations that satisfy such conditions include: 35.8°-Y rotated AT quartz, Euler angles $(0°, -54.2°, 90°)$; ST-90° quartz, Euler angles $(0°, 132.75°, 90°)$; and CdS, Euler angles $(0°, 90°, 0°)$ [9]–[11].

The pure SHSAW is normally weakly guided under free BC, and therefore the use of a guiding structure is typically required in delay-line devices. The guiding structure is intended to concentrate energy near the device surface and reduce shear-horizontal bulk acoustic wave (SHBAW) spurious excitation. Under the effect of further surface guiding, the SHSAW device presents increased sensitivity to surface perturbations [2], [7], thus also improving a sensor's signal-to-noise ratio, dynamic range, and resolution.

High-efficiency excitation of the SHSAW mode by the interdigital transducer (IDT) implies increasing the ratio of the SHSAW power, P_{SHSAW}, with respect to the total interdigital transducer (IDT) input power, P_{in}, $\eta_{SHSAW} = P_{SHSAW}/P_{in}$. Delay line designs having IDTs with η_{SHSAW} near 100% demonstrate reduced generation and detection of SHBAW. The reduced SHBAW interference translates into improved SHSAW phase linearity, again improving the sensor's signal-to-noise ratio, dynamic range and resolution.

Previous work utilizing boundary element method (BEM) techniques on pure shear-horizontal orientations

Manuscript received November 2, 2010; accepted February 17, 2011. Funding for this project was provided by The National Science Foundation (NSF ECS-0134335 and ECS-0329913).

The authors are with the Department of Electrical and Computer Engineering, University of Maine, Orono, ME (e-mail: mdacunha@eece.maine.edu).

Digital Object Identifier 10.1109/TUFFC.2011.1909

of lead zirconate titanate (PZT-4) [12] and potassium niobate ($KNbO_3$) [7] reported η_{SHSAW} for a finite-length IDT with either free of infinitesimally thin uniform guiding electrodes on both sides of the IDT. For these high-electromechanical-coupling materials and orientations the loading effect of finite-thickness electrodes was neglected. For lower-piezoelectric-coupling materials and orientations supporting pure shear horizontal behavior, such as quartz ST-90° or LGS Euler angles $(0°, 22°, 90°)$ [4], referred to as LGS $(0°, 22°, 90°)$ from this point on in this work, the finite electrode thickness cannot be neglected in the wave guiding analysis.

To study the effect of mass loading on η_{SHSAW} for lower electromechanical coupling materials and orientations, a combined finite element method (FEM) and BEM model was used in [13]. Periodic guiding gratings were used in that analysis on both sides of an IDT oriented along the pure SHSAW orientation LGS $(0°, 22°, 90°)$. In the referred work, the finite thickness of all grating electrodes was considered. However, the study did not address the case of uniform electrode guiding.

To consider the mass and stiffness effects of structures consisting of the transducer and a single uniform electrode around the IDT, the BEM formalism would require representation of interfacial wave source fields that extend to $\pm\infty$; e.g., surface normal components of stress and charge density at the semi-infinite electrode/substrate interface. This becomes a problem because an efficient and convergent basis function set representing the source fields for such an electrode/interface domain has yet to be identified. Also, the FEM technique, used to analyze the electrode mass and stiffness of the electrodes, would require a semi-infinite mesh; a numerically unreasonable situation.

In this work, a quarter-wavelength technique is introduced utilizing a FEM/BEM tool which allows the study of a finite-length uniform electrode used to guide the SHSAW and to improve the SHSAW IDT transduction efficiency η_{SHSAW}. The guiding performance of the single finite-length uniform electrode is also compared with two other structures: uniform electrodes on both sides of the IDT and semi-infinite guiding gratings on both sides, as shown in Fig. 1. This work shows that in addition to the different guiding structure topologies depicted in Fig. 1, full consideration of the mass/stiffness effects of all electrodes and surrounding boundary condition is required to accurately determine and improve η_{SHSAW} for SHSAW orientations displaying reduced electromechanical coupling, such as quartz ST-90°. In particular, the analysis presented in this work evaluates η_{SHSAW} for the guiding structures in Fig. 1 as a function of electrode metallization thickness and number of IDT electrodes using the introduced quarter-wavelength technique together with a FEM/BEM tool.

Each structure in Fig. 1 consists of finite thickness electrodes atop a semi-infinite piezoelectric substrate. All structures are assumed to extend infinitely and display no field variation along the y-direction, i.e., $\partial/\partial y = 0$. The finite-length split-finger IDTs depicted in Figs. 1(a) and 1(b) contain a semi-infinite uniform guiding electrode on one or both sides, respectively. In Fig. 1(c), the finite split-finger IDT is surrounded by semi-infinite synchronous guiding gratings on each side with electrode periodicity equal to that of the IDT. The ST-90° orientation of quartz, Euler angles $(0°, 132.75°, 90°)$, is selected for analysis in this work as the SHSAW platform material and orientation. Quartz is relatively inexpensive, well-characterized, and the ST-90° orientation belongs to the previously discussed symmetry type 4 class which supports pure shear-horizontal propagation [8] and displays relatively high phase velocity. Isotropic gold (Au) is assumed to be the electrode material in the analysis because of its applicability in biosensors and its excellent SHSAW surface-guiding capabilities associated with its relatively high density.

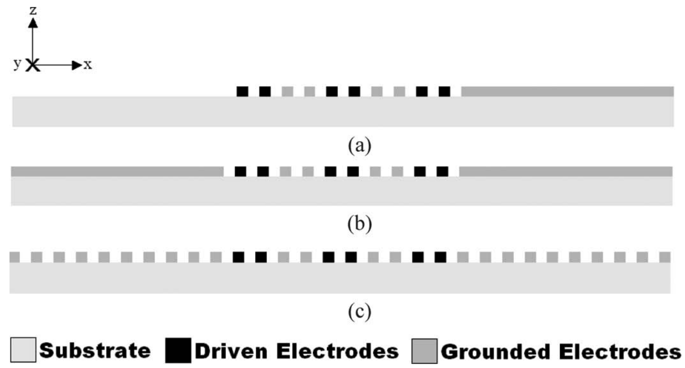

Fig. 1. Single IDT with three guiding boundary conditions: (a) semi-infinite uniform guiding electrode on one side only; (b) semi-infinite uniform guiding electrodes on both sides; and (c) semi-infinite guiding gratings on both sides.

Section II describes the modeling and extraction techniques used for the structures in Fig. 1(a) and 1(b), whereas Section III describes the analysis of the periodic structure in Fig. 1(c). Section IV presents numerical results for the structures in Fig. 1, considering various metallization thicknesses and number of IDT electrodes. Section V compares experimental data to numerical predictions, which validate the proposed method. Section VI is dedicated to conclusions.

II. Uniform Electrode Guiding Evaluation

A. Analysis Approach

To calculate η_{SHSAW} for the structures depicted in Figs. 1(a) and 1(b), a previously implemented FEM/BEM simulation tool is expanded to consider: 1) semi-infinite uniform electrodes on one or both sides of a finite length IDT; and 2) the mass and stiffness effects of all electrodes, including the guiding electrodes. The IDT transduction efficiency is then studied as a function of film metallization thickness and transducer length.

The modified structure considered for the analysis of Fig. 1(a) is shown in Fig 2(a). Instead of studying a semi-infinite electrode, a long truncated electrode is used fol-

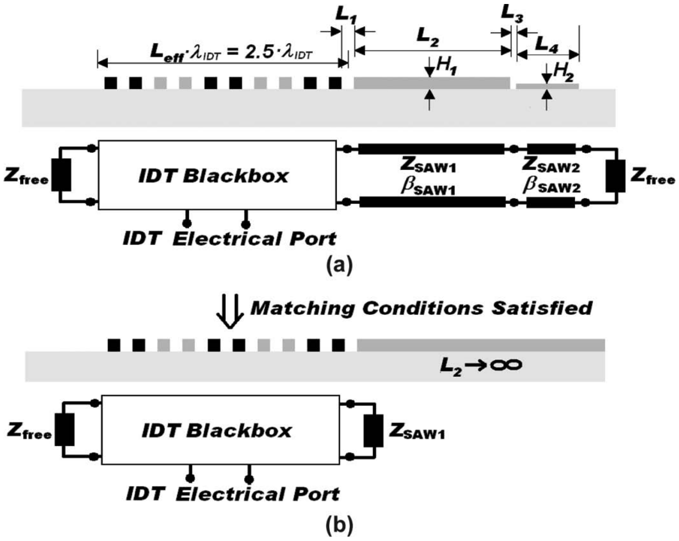

Fig. 2. (a) Truncated structure simulated including a matching electrode and the analogous transmission line representation (where λ_{IDT} is the IDT periodicity). Represented in the figure, $L_{\mathrm{eff}} = 2.5$. (b) Equivalent structure and transmission line representation when the quarter-wave transformer matching requirement is met.

lowed by an additional matching electrode placed directly after the guiding structure. The uniform long guiding electrode cannot be simply truncated without the incorporation of the matching electrode because acoustic reflections from the electrode edge discontinuity normally interact strongly with the launching IDT, making it difficult to estimate the IDT input power of the referred structure. Through the adjustment of the matching electrode dimensions, namely the film thickness and length, the reflected SHSAW at the truncated electrode can be effectively canceled. As a result, the IDT input admittance and the magnitude of the guided SHSAW mode along the truncated electrode region can be estimated as if the electrode extended infinitely. In addition to the structure simulated, Fig. 2(a) shows an analogous transmission line representation. If the truncated electrode of length L_2 and thickness H_1 is long relative to wavelength, only the guided SHSAW is present at the surface far away from the IDT. Such a situation can be modeled as an electromagnetic wave propagating on a transmission line having characteristic impedance Z_{SAW1} and propagation constant $\beta_{\mathrm{SAW1}} = \omega \cdot s_{\mathrm{SAW1}}$, where ω is the radian frequency and s_{SAW1} is the inverse velocity or slowness of the SHSAW for the analogous uniform-layer over a semi-infinite substrate propagation condition. The matching electrode of length L_4 and thickness H_2 is modeled in the same way, and has characteristic impedance Z_{SAW2} and propagation constant $\beta_{\mathrm{SAW2}} = \omega \cdot s_{\mathrm{SAW2}}$. The load impedance Z_{free} is analogous to the impedance looking toward the free surface. The matching technique employed in this work is analogous to transmission line quarter-wave transformer theory. It is shown that by altering H_2, the effective Z_{SAW2} is modified, and by varying L_4, the effective electrical length is modified. Thus, by adjusting each parameter, the quarter-wave transformer matching criterion

$$Z_{\mathrm{SAW2}} = \sqrt{Z_{\mathrm{SAW1}} \cdot Z_{\mathrm{free}}}, \quad L_4 = \frac{\pi}{2 \cdot \beta_{\mathrm{SAW2}}}(1 + 2 \cdot n) \quad (1)$$

can be satisfied, where n is a nonnegative integer. Under this condition, the SHSAW reflected power at the truncated electrode edge is cancelled at a particular frequency, and the structure behaves as if the electrode extends infinitely, as indicated in Fig. 2(b).

B. Procedure for Matching Electrode Determination and Power Ratio Calculation

A case study is given in this section to demonstrate the η_{SHSAW} calculation technique based on the structure defined in Fig. 2(a). The split-finger IDT under consideration consists of 4-µm electrodes, $L_{\mathrm{eff}} = 4.5$, IDT periodicity, $\lambda_{\mathrm{IDT}} = 32$ µm, 1:1 mark-to-space ratio, $L_1 = 4$ µm, $L_2 = 800$ µm, $L_3 = 2$ µm, L_4 = variable (varying from 33.5 to 36.5 µm), $H_1 = 300$ nm, and H_2 = variable (varying from 190 to 260 nm). The IDT has acoustic aperture $W = 1600$ µm and is oriented along quartz ST-90°.

For all FEM/BEM simulations presented in this work, the following basis functions are used to approximate the interfacial surface-normal stress components and charge density at an electrode/substrate interface [14]–[16]:

$$f^{mn}(x) = \left\{ \begin{matrix} \dfrac{T_n\left(\frac{x-c_m}{a_m}\right)}{\sqrt{1-\left(\frac{x-c_m}{a_m}\right)^2}} & c_m - a_m \le x \le c_m + a_m \\ 0 & \text{otherwise} \end{matrix} \right\}, \quad (2)$$

where for a particular f^{mn} basis function, T_n is the nth-order Chebyshev polynomial of the first kind; c_m is the center position of the mth electrode; and a_m is the half-length of the mth electrode. The definitions for the Fourier and inverse Fourier transform adopted in this work are given by

$$\bar{f}(k_x) = \frac{1}{2\pi} \int_{-\infty}^{\infty} f(x) e^{jk_x x} \mathrm{d}x \quad (3a)$$

$$f(x) = \int_{-\infty}^{\infty} \bar{f}(k_x) e^{-jk_x x} \mathrm{d}k_x, \quad (3b)$$

and the spectral-domain representation of (2) is given by

$$\overline{f^{mn}}(k_x) = \frac{1}{2} j^n a_m J_n\left(a_m k_x\right) e^{jk_x c_m}, \quad (4)$$

where $k_x = \omega \cdot s_x$ is the x-directed wavenumber, s_x is x-directed inverse velocity or slowness, and J_n is the nth-order Bessel function of the first kind.

To consider the electrode mass/stiffness behavior, the FEM technique is used to determine the interfacial mesh nodal forces and displacements by employing a uniform-density mesh consisting of 8-node square elements subject to the stress distributions at the interface given by (2). Next, the particle displacement distribution at an electrode interface is multiplied by the basis functions and integrated over an electrode's domain to allow coupling to the BEM model and determination of the stress and charge fields at the interface for a given potential at the electrodes [14].

Using the aforementioned FEM/BEM tool and dimensions of the design considered in this case study, the Chebyshev basis function in (2) of orders up to 12, 100, and 20, were used for the 4-μm IDT electrodes, 800-μm uniform guiding electrode, and 35-μm matching electrode, respectively. The analysis showed that polynomials of these orders were adequate to guarantee convergence within the IDT bandwidth. As the length of the guiding electrode increases, the dominant functional dependence of the stress and charge fields far away from the IDT and along the uniform guiding electrode resemble that of a SHSAW propagating wave. By expanding this field variation with a weighted series of basis functions given by (2), the respective coefficients can be determined using the orthogonality properties of the Chebyshev polynomials. Given the coefficients' functional dependence with the polynomial order, an expression can be determined for the estimation of the required polynomial order to describe the SHSAW field behavior. This analysis showed that the required number of basis functions to describe the fields can be estimated by ceiling$\{1.25\cdot\pi\cdot L_2/\lambda_{\mathrm{g}}\}$, where λ_{g} is the SHSAW acoustic wavelength along the guiding electrode region.

The next step in the η_{SHSAW} calculation is the determination of the excitation frequency for the analysis. In this work, the frequency of maximum IDT conductance was selected as the excitation frequency. The structure in Fig. 1(c) was used for the determination of the approximate frequency of maximum IDT conductance, and yielded in this work, for the dimensions mentioned at the beginning of this section, a device center frequency of 150.8 MHz.

To proceed with the η_{SHSAW} calculation, the fields along the guiding electrode interface associated with SHSAW need are extracted from the FEM/BEM results. In particular, $P^{+}{}_{\mathrm{SHSAW}}$ and $P^{-}{}_{\mathrm{SHSAW}}$, which stand for the power of the forward and backward SHSAW under the truncated electrode region, respectively, are extracted.

The FEM/BEM calculated fields along the truncated electrode interface include contributions from electrostatic effects, SHBAW, evanescent modes, and the SHSAW. The SHSAW shear-horizontal fields—namely, the surface normal component of stress, T_4, or the charge density, σ—can be extracted from the total contribution via Fourier transform spectral-domain fitting. For the SHSAW field fitting, T_4 was preferred over σ, because the electrostatic part of σ may have a significant contribution which makes it more difficult to extract the SHSAW contribution. Such an effect is not present in T_4, and the SHSAW contribution dominates the overall field behavior over the entire structure shown in Fig. 2.

The fitting procedure is performed as follows. Considering only the SHSAW, and neglecting any other field contribution caused by electrostatics or other modes, the fitting technique assumes that T_4 along the truncated electrode/substrate interface is given as a weighted sum of $+x$ and $-x$ propagating waves having velocity equal to that for the guided SHSAW, i.e.,

$$\begin{aligned} T_4(x) = {} & (T_4^{+} e^{-j\beta_{\mathrm{SAW1}}(x-c-a)} + T_4^{-} e^{j\beta_{\mathrm{SAW1}}(x-c-a)}) \\ & \cdot [U(x-c+a) - U(x-c-a)], \end{aligned} \tag{5}$$

where c is the center position of the truncated electrode, a is the half-length of the truncated electrode, and U is the unit-step function. $T_4{}^{+}$ and $T_4{}^{-}$ are the unknown weights associated with the $+x$ and $-x$ propagating SHSAW, respectively. Using (3), the spectral-domain representation of (5) is given by

$$\begin{aligned} \overline{T_4}(k_x) = {} & T_4^{+} e^{j(k_x c + \beta_{\mathrm{SAW1}} a)} \frac{\sin[a(k_x - \beta_{\mathrm{SAW1}})]}{\pi(k_x - \beta_{\mathrm{SAW1}})} \\ & + T_4^{-} e^{j(k_x c - \beta_{\mathrm{SAW1}} a)} \frac{\sin[a(k_x + \beta_{\mathrm{SAW1}})]}{\pi(k_x + \beta_{\mathrm{SAW1}})}. \end{aligned} \tag{6}$$

An estimation of $T_4{}^{+}$ and $T_4{}^{-}$ is obtained by fitting (6) at $k_x = \pm\, \beta_{\mathrm{SAW1}}$ to the computed $\overline{T_4}(k_x)$ contribution, considering only the $T_4(x)$ field along the long guiding electrode, which is determined using (4) and the results of the FEM/BEM analysis. Finally, the power associated with the forward and backward propagating SHSAW, $P^{+}{}_{\mathrm{SHSAW}}$, and $P^{-}{}_{\mathrm{SHSAW}}$, are determined through integration of the x-directed Poynting vector along the entire z-axis, from $-\infty$ to the top surface of the electrode. The reflection coefficient looking into the matching electrode region, $|\Gamma_{\mathrm{SHSAW}}| = |P^{-}{}_{\mathrm{SHSAW}}/P^{+}{}_{\mathrm{SHSAW}}|^{1/2}$, can also be estimated, and is used to quantify the degree of matching achieved.

At the selected frequency and using the technique described, simulations were performed for a combined range of L_4 and H_2. The thickness and length of the matching electrode were varied over a range of ± 15% and ± 5%, respectively, from their initial values. The thickness H_2 was varied first, because that requires only the FEM analysis for the matching electrode to be recomputed, which typically runs much faster than the BEM analysis. When L_4 is modified, only the affected IDT, guiding, and matching electrode interactions of the BEM matrix are recomputed in order to speed up the calculation.

For the example considered in this section, Fig. 3 shows the computed $|\Gamma_{\mathrm{SHSAW}}|$ for a variety of matching electrode lengths and thicknesses. As can be inferred from Fig. 3, a matching condition is achieved when $L_4 = 34$ μm and $H_2 = 244.2$ nm. Using these dimensions of the matching electrode, the far-field SHSAW power is estimated using the calculated value of $P^{+}{}_{\mathrm{SHSAW}}$ as previously detailed in this section. In addition, the IDT input power is computed, given the calculated IDT input conductance and the applied voltage. From $P^{+}{}_{\mathrm{SHSAW}}$ and P_{in}, one calculates η_{SHSAW}. For the example discussed in this section,

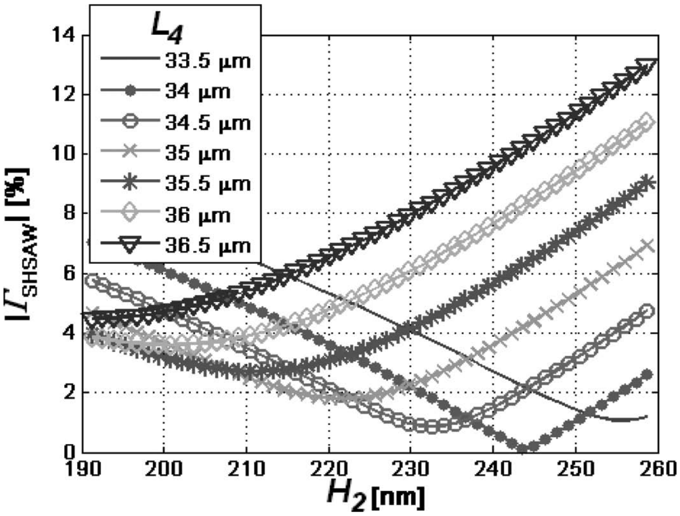

Fig. 3. Magnitude of SHSAW reflection coefficient $|\Gamma_{\mathrm{SHSAW}}|$ as a function of matching electrode length and thickness for the case study considered.

$P^{+}_{\mathrm{SHSAW}} = 2.549\ \mu\mathrm{W}$ (1 V applied) and the IDT input admittance when matched equals 1.186e-5 + j5.155e-4 S. The η_{SHSAW} for the structure in Fig. 2(a) is thus estimated to be 43%, with the entire SHSAW energy propagating under the long guiding electrode, because no SHSAW propagates to the other free-surface side of the IDT for quartz ST-90°.

The effect of the matching electrode can be further appreciated in Fig. 4, where T_4 along the electrode/substrate interface at the IDT and at the long uniform guiding electrode is plotted when the matching electrode is omitted and present in Figs. 4(a) and 4(b), respectively (1 V applied). Fig. 4(c) plots T_4 near the matching electrode when the matching structure is present. As can be seen from Fig. 4(a), the omission of the matching electrode results in a standing wave along the long guiding electrode region; however, when the matching electrode with proper dimensions is included, no standing wave pattern is evident, which indicates a SHSAW matched condition. For the matched case, the field behavior along the long guiding electrode region resembles that of a SHSAW propagating wave under uniform media as one looks further away from the IDT. This indicates the SHSAW is dominant along the truncated electrode region and thus the field amplitudes can be considered as far-field values, and thus are appropriate to calculate η_{SHSAW}. In addition, it is interesting to note from Fig. 4(c) that the effective electrical length of the matching electrode is approximately 1 and 1/4 wavelengths according to the stress variation, which is in accordance with the quarter-wave transformer requirement discussed in (1), Section II-A.

If the guiding structure is considered on both sides of the IDT, the aforementioned analysis is performed twice to determine the required matching electrode dimensions for each side. Once both matching electrodes are determined, simulation is performed including both matching structures, and η_{SHSAW} for each side is extracted using the technique described previously.

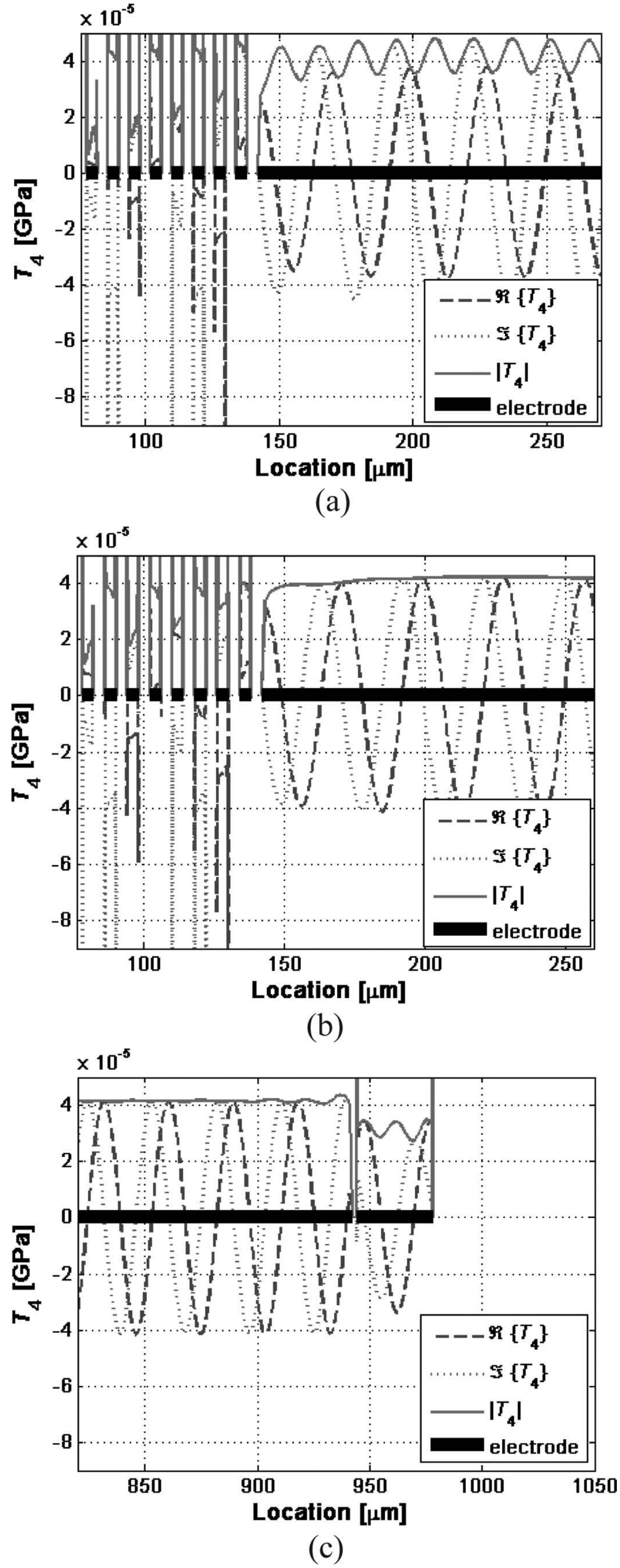

Fig. 4. Resulting interfacial T_4 around the long guiding electrode region when (a) matching electrode is omitted (close to IDT); (b) matching electrode is included in the analysis (close to IDT); (c) matching electrode is included (close to the matching electrode). (1V applied).

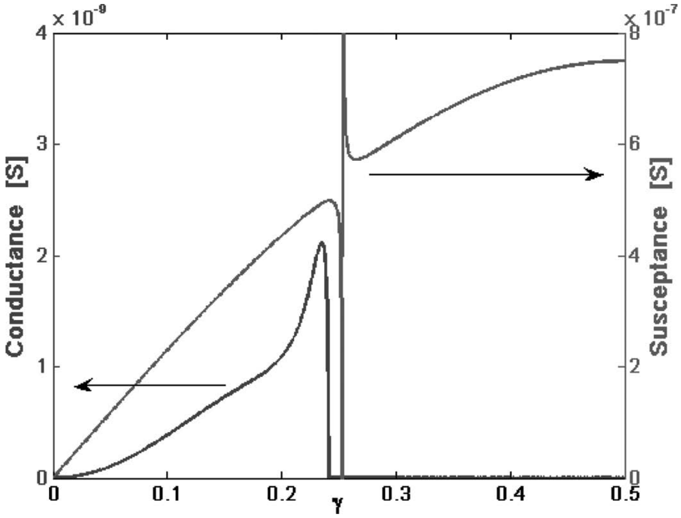

Fig. 5. Computed harmonic admittance $Y(\gamma,\omega)$ for the IDT referred to in the text along quartz ST-90° at 150.8 MHz.

III. Grating Guiding Evaluation

A. Analysis Approach

A periodic full-wave FEM/BEM model was used to evaluate the structure in Fig. 1(c), where guiding gratings surround a finite length IDT to determine η_{SHSAW}. The purpose of this analysis is to provide a comparison to the η_{SHSAW} results obtained when alternative semi-infinite uniform electrode guiding is considered. Periodic tools have been reported [15]–[17], and were extended in previous work by the authors [13] to allow the determination of η_{SHSAW}. In particular, the analysis relies on computation of the harmonic admittance, mutual admittance, and calculation of the IDT input power contribution from the guided SHSAW mode.

In this work, the charge and stress fields at the electrode/substrate interface are approximated using the basis function set given by (2) in Section II. The FEM analysis for the electrode is also treated in the same manner as described in Section II.

B. Power Ratio Extraction Procedure and Example

As an example, the same IDT structure and substrate studied in Section II will now be analyzed for the guiding gratings structure, depicted in Fig. 1(c). The first step in the analysis is to determine the harmonic admittance function $Y(\gamma,\omega)$, where $\gamma = \beta{\cdot}p/(2\pi)$, $\beta{\cdot}p$ is excitation phase difference between adjacent electrodes in the infinite periodic structure, and p is the periodicity of the grating. Fig. 5 shows the computed $Y(\gamma,\omega)$ over a range of $\gamma = [0, 0.5]$ at a simulation frequency of 150.8 MHz; results are normalized to an aperture equal to $p = 8$ µm. It can be shown that $Y(\gamma,\omega)$ is a periodic function with respect to γ, having period equal to 1, and is also symmetric with respect to the $\gamma = 0$ axis. By taking the inverse Fourier series of $Y(\gamma,\omega)$ the mutual admittance $y_m(\omega)$ is obtained as

$$y_m(\omega) = \int_{-1/2}^{1/2} Y(\gamma,\omega) e^{-j2\pi\gamma m} \mathrm{d}\gamma, \tag{7}$$

which is then used to determine the finite-IDT/grating structure input admittance via superposition. In particular, the mutual admittance gives the current entering an electrode m periods away from a single driven electrode (1 V applied, all other electrodes grounded). From (7), the far-field contribution ($|m| \gg 1$) to the mutual admittance is due to the presence of poles in $Y(\gamma,\omega)$, seen in Fig. 5 (near $\gamma = 0.25$), whose locations correspond to the SHSAW short-circuit grating mode. The linear transformation of (7) allows the separation of the mutual admittance into contributions from the SHSAW mode and a residual component, which includes electrostatic and SH-BAW effects. The mutual admittance contribution from the SHSAW grating mode is determined by fitting the poles in $Y(\gamma,\omega)$ to an analytical function, then integrating analytically, whereas the residual contribution is determined via numerical integration [13], [17]. The SHSAW power contribution can be found from the determined SHSAW contribution to the mutual admittance, and resulted in this example in a power ratio of 90.8%. Because of reciprocity, it can be shown that $y_m = y_{-m}$ [17], which results in non-directional excitation for the structure considered, thus equal SHSAW power is excited for both forward and reverse propagation directions.

IV. Numerical Analysis

A. Uniform Electrode Guiding Results

Based on the extraction technique presented in Section II, η_{SHSAW} for finite-length split-finger IDTs with semi-infinite uniform guiding electrodes on one and both sides of the IDT were determined for various metallization thicknesses and number of IDT split-finger pairs. The analysis was carried out for quartz ST-90°, Au metallization, split-finger IDT with 4-µm electrodes, $\lambda_{\mathrm{IDT}} = 32$ µm, and mark-to-space ratio = 1:1; and with all guiding electrodes connected to the IDT ground. The structures studied consisted of IDTs with $L_{\mathrm{eff}} = 4.5$, 9.5, 19.5, 39.5, and 79.5, and $H_1 = 75$, 150, 300, and 600 nm. L_1 and L_3 were chosen to be 4 µm and 2 µm, respectively. L_2 was selected as 800 µm and 1200 µm, and verified that the difference between extracted η_{SHSAW} was less than 1% for increased guided electrode length. Thus, 800 µm was adopted as a long enough guiding structure for this analysis such that if increased the extracted value of η_{SHSAW} would be affected by less than a percent. The percent variation is then considered the uncertainty for the η_{SHSAW} results presented in this section.

Fig. 6 shows the results of the computed η_{SHSAW} for the structures represented in Fig. 1 as a function of L_{eff} considering diverse electrode metallization thicknesses. In

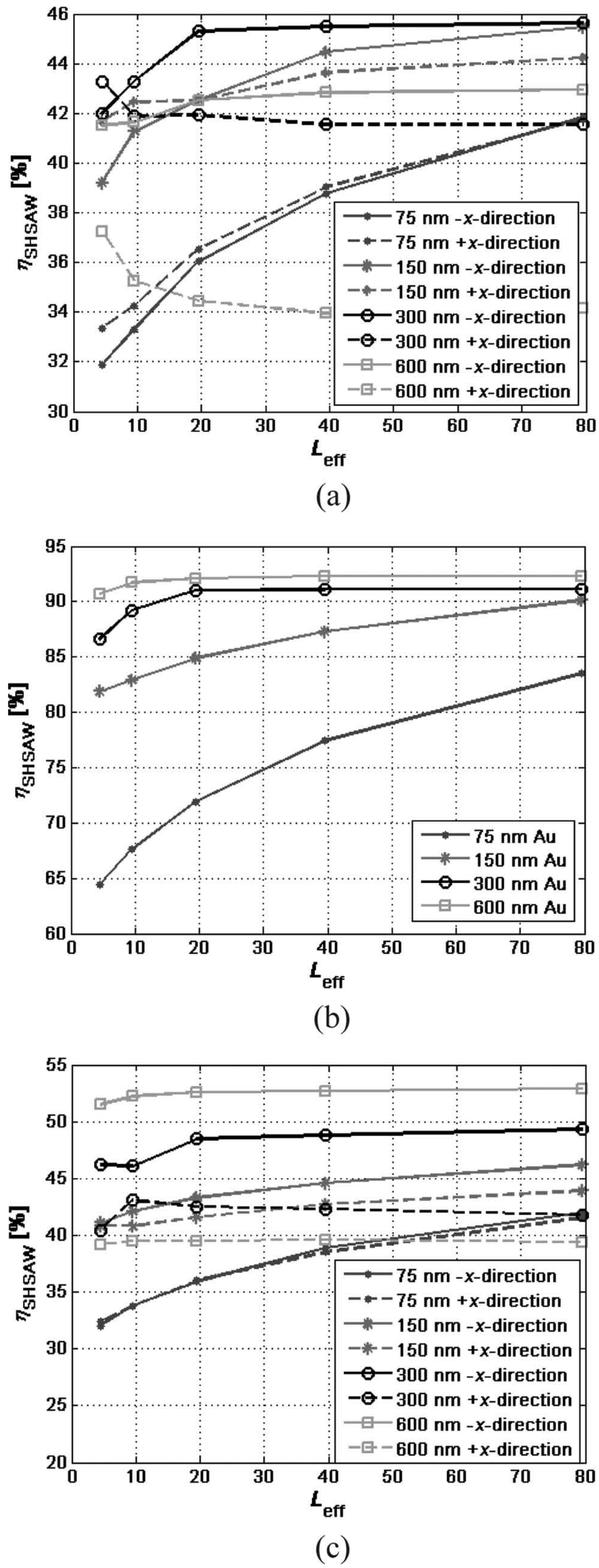

Fig. 6. SHSAW excitation efficiency η_{SHSAW} [%] for split-finger IDTs of different lengths and metallization thicknesses under the matched condition: (a) single uniform guiding electrodes on the left and right side of IDT, (b) uniform guiding electrodes on both sides of IDT and total left and right propagated SHSAW, and (c) uniform guiding electrodes on both sides of IDT with separated left and right propagating SHSAW contributions.

particular, Fig. 6(a) shows η_{SHSAW} for the structure represented in Fig. 1(a) where a single semi-infinite uniform electrode is on one side of the IDT, as well as the reverse situation. Fig. 6(b) gives η_{SHSAW} for the structure represented in Fig. 1(b), where the guiding electrodes are on both sides of the IDT. Finally, Fig. 6(c) plots η_{SHSAW} split into both $+x$- and $-x$-propagating SHSAW contributions, again for the structure represented in Fig. 1(b). The results shown in Fig. 6(b), indicate that the overall η_{SHSAW}, considering excitation to both sides, increases with IDT length toward an asymptotic value, and also increases with metallization thicknesses. Within the previously assumed 1% uncertainty, Fig. 6(a) shows that η_{SHSAW} increases with thickness up to a 300-nm-thick Au film, and then the efficiency decreases for the thicker 600-nm film. This behavior might be credited to the higher structural mismatch between the IDT region with thicker electrodes and the free region, which then leads to more power transduced into the SHBAW for the ST-90° orientation. Fig. 6(a) also reveals an interesting directivity effect which takes place for thicker films. For thinner films, the placement of the long electrode on the left or the right of the IDT generates comparable η_{SHSAW} performance. For the thicker electrodes, in particular for 600-nm-thick electrodes, about 9% difference in excitation between forward and backward propagation is identified when the electrodes are positioned on one side or the other of the IDT. A similar directivity effect for thicker electrodes is observed on Fig. 6(c), where long electrodes are present on both sides of the IDT and split into contributions to each side. Comparing Figs. 6(a) and 6(c), one can see that for a selected thickness, the presence of long electrodes on both sides of the IDT increases the overall SHSAW excitation for both the forward and backward propagation directions when compared with having the electrodes on one side only. The effect is more pronounced for the thicker 600-nm-electrode case. The higher overall η_{SHSAW} for the quartz ST-90° case in which electrodes are present on both sides is justifiable by less SHBAW excitation and SHSAW excitation on both directions, as opposed to a single direction in the case of electrode on only one side.

B. Guiding Grating Results

Based on the extraction technique presented in Section III, η_{SHSAW} was computed for the same finite-length split-finger IDTs and metallization thicknesses considered in subsection *A*, but with guiding gratings on both sides of the IDT instead. Fig. 7 gives the extracted η_{SHSAW} analysis for the structure represented in Fig. 1(c) as a function of L_{eff} and considering diverse electrode metallization thicknesses. Fig. 8 reveals that η_{SHSAW} approaches 100% for shorter IDTs if thicker electrodes are used. In addition, the use of guiding gratings results in η_{SHSAW} approaching 100%, whereas when guiding uniform electrodes were considered (Fig. 6), η_{SHSAW} approaches values less than 100%. This result indicates that the guiding gratings provide higher η_{SHSAW}, and thus less SHBAW scattering and

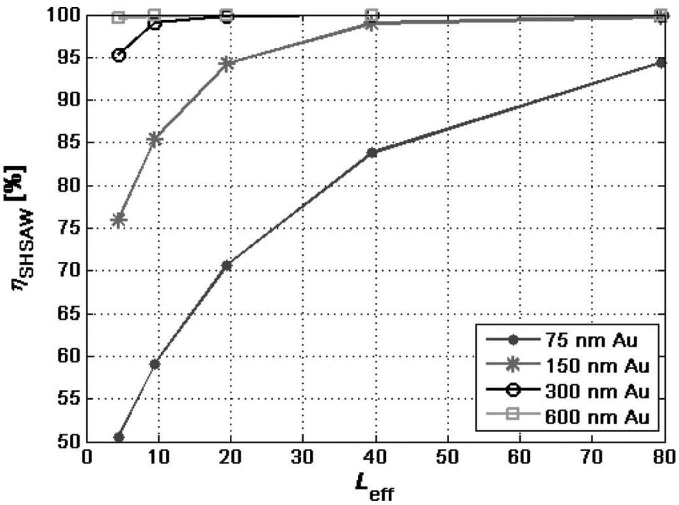

Fig. 7. SHSAW excitation efficiency η_{SHSAW} [%] for split-finger IDTs of different lengths and metallization thicknesses, when infinite guiding gratings are considered.

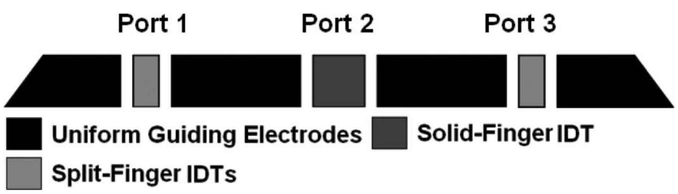

Fig. 8. Layout of the SHSAW device fabricated.

acoustic reflections caused by structure discontinuities which take place for the long electrode cases.

V. Experimental Verification

To experimentally verify the proposed modeling technique, and in particular the directivity effect reported in the previous section, a quartz ST-90° delay-line structure consisting of a regular two-electrodes per wavelength IDT, two identical split-finger IDTs, and long guiding uniform electrodes were fabricated as shown in Fig. 8. The structure was simulated and the results were compared with measurements. The structure shown in Fig. 8 allows the determination of P_{SHSAW} going to the left with respect to P_{SHSAW} going to the right excited by the Port 2 IDT and defined as directivity D_{solid}.

The fabricated device consists of a two-electrode per wavelength input IDT having L_{eff} = 79.5, λ_{IDT} = 32 µm, 8-µm electrodes, and mark-to-space ratio = 1:1. Long uniform guiding electrodes, with 6 µm gaps between themselves and the extreme solid-finger IDT electrodes, extend 9596 µm in each direction. The split-finger IDTs have L_{eff} = 39.5, λ_{IDT} = 32 µm, 4-µm electrodes, mark-to-space ratio = 1:1, and 4 µm gaps between themselves and the guiding electrodes. On the other side of the split-finger IDTs, long uniform guiding electrodes approximately 6500 µm in length are placed 4 µm from the outer edge of each IDT. The guiding electrodes are terminated with a

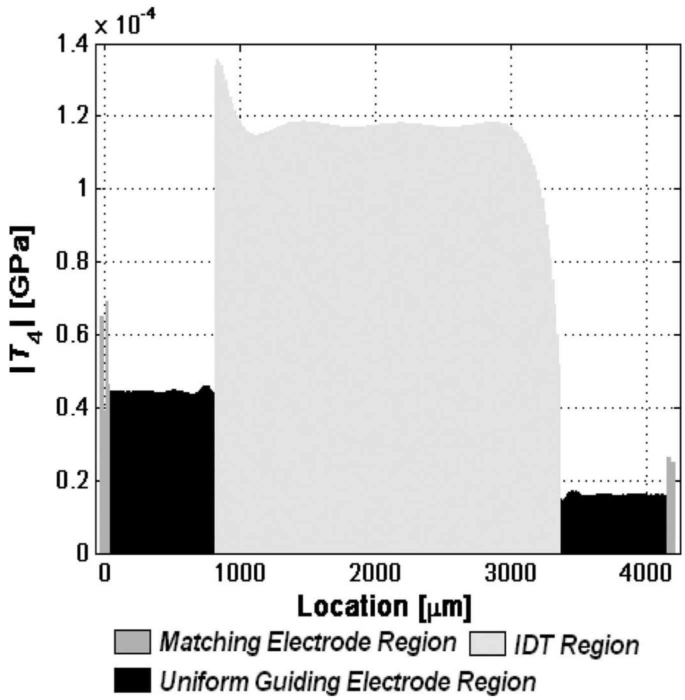

Fig. 9. Calculated $|T_4|$ along electrode/substrate interface for the solid-finger IDT including guiding and matching electrodes.

diagonal edge to scatter reflections. The acoustic aperture of the device is 1600 µm. The Au metallization layer is 287.5 nm thick atop a 10-nm Cr adhesion layer. Devices were fabricated at the Laboratory for Surface Science & Technology (LASST) clean room facility and tested at the Microwave Acoustics Laboratory at the University of Maine.

The input transducer, Port 2, was numerically analyzed using the technique described in Section II, considering uniform guiding electrodes on both side of the two-electrodes per wavelength IDT and inclusion of matching electrodes. Fig. 9 shows the calculated $|T_4|$ at the interface after the matching described in Section II (1 V applied). The analysis and Fig. 9 clearly reveals a directional behavior of the Port 2 IDT because P^{+}_{SHSAW} and P^{-}_{SHSAW} are both proportional to $|T_4|^2$ associated with the forward and backward propagating SHSAW. Based on the calculated P^{+}_{SHSAW} and P^{-}_{SHSAW} along the uniform guiding electrode/substrate interface, the directivity for the structure is determined to be 9.0 dB.

Fig. 10 plots the measured $|S_{12}|$ and $|S_{32}|$ obtained for both the forward and backward delay-line propagation directions on quartz ST-90° with Au electrodes, H_1/λ_{IDT} = 0.9%. As expected based on the previous analysis using the proposed model, the natural single-phase unidirectional transducer (NSPUDT) directivity effect is experimentally observed.

To compare the experimental results shown in Fig. 10 with predicted D_{solid} results, the finite directivity of the split-finger detection IDTs, D_{split}, are considered and estimated from Fig. 6(c) to be 0.4 dB for a 300-nm thick film. Minor differences in the $|S_{11}|$ and $|S_{33}|$ frequency respons-

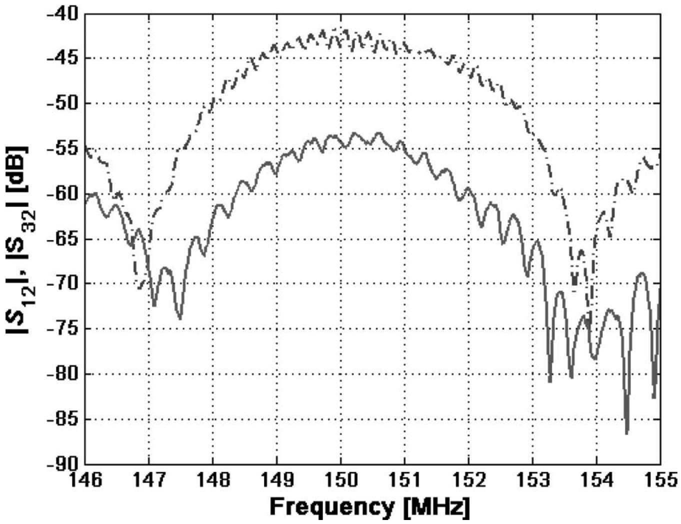

Fig. 10. Experimentally measured $|S_{12}|$ (dot-dashed line) and $|S_{32}|$ (solid line) for the NSPUDT device fabricated demonstrating ST-90° directionality. Port 2 is connected to the solid-finger IDT and Ports 1 and 3 are connected to the split-finger IDTs as shown in Fig. 8.

es for the two split-finger IDTs have been measured and considered in the analysis. After time-gating to remove spurious reflections, the minimum measured value of $|S_{11}|$ was about -0.71 dB at 150 MHz compared -0.63 dB at 150.8 MHz for $|S_{33}|$. These observed small variations in frequency response between the two IDTs (about 1 MHz in 150 MHz) was credited to variations in the fabrication process, namely the thin film thickness and the patterned mark-to-space ratio for the structure built. To account for the observed fabrication variation toward the extraction of D_{solid}, a relative port efficiency factor defined as $\delta = (1 - |S_{11}|^2)/(1 - |S_{33}|^2)$ was computed, which relates the efficiency of acoustic excitation/detection between Port 1 and Port 3 IDTs. Finally, D_{solid} is calculated by $D_{\text{solid}} = D_{\text{split}} \cdot (|S_{12}|^2/|S_{32}|^2)/\delta$ and at 150 MHz resulted in 9.8 dB.

Therefore, the proposed model successfully predicts the experimentally observed directivity effect for the pure SHSAW on quartz ST-90° with Au electrodes. The calculated and measured directivity agree within 0.8 dB for 9 dB experimentally measured, which is reasonable given the uncertainties and variations in the fabricated structure parameters and choices for the extrapolated D_{split} used in the calculations.

VI. Conclusions

In this work, guiding uniform electrode and grating structures placed next to a finite-length IDT were studied using numerical techniques to determine how the ratio of transduced guided SHSAW power to IDT input power can be improved.

A novel matching electrode technique was introduced in the simulation of a finite-length structure, via finite FEM/BEM model, to simulate an acoustically matched, infinite structure. It has been quantitatively verified that long guiding electrodes on both sides of the IDTs, as opposed to only between the IDTs, can cause up to 45% improvement in the achievable SHSAW transmission magnitude for a delay line fabricated along the ST-90° orientation of quartz. This work also revealed that long and thick IDTs with guiding gratings, as opposed to uniform guiding electrodes, results in up to 8% higher SHSAW transduction efficiency. However, short and thin IDTs with uniform guiding electrodes can provide up to 15% higher efficiency than the use of gratings.

Experimental devices were fabricated on quartz ST-90° to verify the NSPUDT directivity effect that was revealed by the analysis carried out in this work for the pure SHSAW devices with heavier gold electrodes. The experimental verification of the predicted directivity effect for the uniform finite-thickness Au guiding electrodes surrounding a solid-finger IDT confirmed the adequacy of the proposed model.

References

[1] T. M. A. Gronewold, "Surface acoustic wave sensor in the bioanalytical field: Recent trends and challenges," *Anal. Chim. Acta*, vol. 603, no. 2, pp. 119–128, Nov. 2007.

[2] K. Länge, B. E. Rapp, and M. Rapp, "Surface acoustic wave biosensors: A review," *Anal. Bioanal. Chem.*, vol. 391, no. 5, pp. 1509–1519, Jul. 2008.

[3] J. C. Andle and J. F. Vetelino, "Acoustic wave biosensors," in *Proc. IEEE Ultrasonics Symp.*, 1995, pp. 451–460.

[4] M. Pereira da Cunha, D. C. Malocha, D. W. Puccio, J. Thiele, and T. B. Pollard, "LGX pure shear horizontal SAW for liquid sensor applications," *IEEE Sens. J.*, vol. 3, no. 5, pp. 554–561, Oct. 2003.

[5] J. Kondoh and S. Shiokawa, "Measurements of conductivity and pH of liquid using surface acoustic wave devices," *Jpn. J. Appl. Phys.*, vol. 31, suppl. 31–1, pp. 82–84, 1992.

[6] E. Gizeli, A. C. Stevenson, N. J. Goddard, and C. R. Lowe, "A novel Love-plate acoustic sensor utilizing polymer overlayers," *IEEE Trans. Ultrason. Ferroelectr. Freq. Control*, vol. 39, no. 5, pp. 657–659, Sep. 1992.

[7] T. B. Pollard, T. D. Kenny, J. F. Vetelino, and M. Pereira da Cunha, "Pure SH-SAW propagation, transduction, and measurements on $KNbO_3$," *IEEE Trans. Ultrason. Ferroelectr. Freq. Control*, vol. 53, pp. 199–208, Jan. 2006.

[8] G. W. Farnell and E. L. Adler, "Elastic wave propagation in thin layers," in *Physical Acoustics*, vol. 9, W. P. Mason and R. N. Thurston, Ed. New York, NY: Academic Press, 1972, pp. 35–127.

[9] J. L. Bleustein, "A new surface wave in piezoelectric materials," *Appl. Phys. Lett.*, vol. 13, no. 12, pp. 412–413, Dec. 1968.

[10] M. Lewis, "Surface skimming bulk waves—SSBW," in *Proc. IEEE Ultrasonics Symp.*, 1977, pp. 744–752.

[11] K. H. Yen, K. F. Lau, and R. S. Kagiwada, "Recent advances in shallow bulk wave devices," in *Proc. IEEE Ultrasonics Symp.*, 1979, pp. 776–785.

[12] R. F. Milsom, N. H. C. Reilly, and M. Redwood, "Analysis of generation and detection of surface and bulk acoustic wave by interdigital transducers," *IEEE Trans. Sonics Ultrason.*, vol. SU-24, pp. 147–166, May 1977.

[13] T. B. Pollard and M. Pereira da Cunha, "Improved pure SH SAW transduction efficiency on LGS using finite thickness gratings," in *Proc. IEEE Ultrasonics Symp.*, 2005, pp. 1048–1051.

[14] P. Ventura, J. M. Hodé, and B. Lopes, "Rigorous analysis of finite SAW devices with arbitrary electrode geometries," in *Proc. IEEE Ultrasonics Symp.*, 1995, pp. 257–262.

[15] P. Ventura, J. M. Hodé, J. Desbois, and M. Solal, "Combined FEM and Green's function analysis of periodic SAW structure, application to the calculation of reflection and scattering parameters," *IEEE Trans. Ultrason. Ferroelectr. Freq. Control*, vol. 48, pp. 1259–1274, Sep. 2001.

[16] V. P. Plessky and T. Thorvaldsson, "Periodic Greens's function analysis of SAW and leaky SAW propagation in a periodic system of electrodes," *IEEE Trans. Ultrason. Ferroelectr. Freq. Control*, vol. 42, pp. 280–293, Mar. 1995.

[17] Y. Zhang, J. Desbois, and L. Boyer, "Characteristic parameters of surface acoustic waves in a periodic metal grating on a piezoelectric substrate," *IEEE Trans. Ultrason. Ferroelectr. Freq. Control*, vol. 40, pp. 183–192, May 1993.

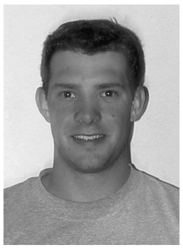

Thomas Bain Pollard (S'02) was born in Blue Hill, ME, on October 29, 1979. He received the B.S. degree in computer engineering from the University of Maine, Orono, Maine, in 2003 and is completing his Ph.D. degree with the Department of Electrical and Computer Engineering at the University of Maine. He is currently a Principal Engineer with Environetix Technologies Corporation, Orono, ME. He worked on microwave acoustics research at the Microwave Acoustics Laboratory at the University of Maine's Laboratory for Surface Science and Technology (LASST) from 1999 to 2010. As an undergraduate student, he was a three-time participant in the National Science Foundation Research Experience for Undergraduates (NSFREU) summer program at the University of Maine. His current research interests are harsh environment SAW sensor design and characterization, SAW liquid-phase biosensors, new materials, shear horizontal SAW, and interdigital transducer modeling.

T. B. Pollard is a student member of the IEEE Ultrasonics, Ferroelectrics, and Frequency Control Society (UFFC). He has twice been a student paper competition finalist, at the 2003 and 2004 Utrasonics Symposia.

Mauricio Pereira da Cunha (S'88–M'95–SM'02) was born in Brazil in 1963, received a bachelor's degree in 1985, and a master's degree with honors in electrical engineering in 1989, from the Escola Politécnica, Universidade de São Paulo. His master's thesis title is "Design and Implementation of a 70 MHz SAW Convolver." He received the Ph.D. degree, Dean's Honor List, from McGill University, Montreal, PQ, Canada, in electrical engineering in 1994. His Ph.D. thesis title is "SAW Propagation and Device Modeling on Arbitrarily Oriented Substrates."

Mauricio has worked with the Microwave Devices R&D Group at NEC (Nippon Electric Co.), Brazil, Laboratório de Microeletrônica, Escola Politécnica, Department of Electrical Engineering, Universidade de São Paulo, McGill University, Montreal, PQ, Canada, and SAWTEK Inc., Orlando, FL. He spent a sabbatical year at University of Central Florida, Consortium for Applied Acoustoelectronic Technology (CAAT), Orlando, FL, where he worked in cooperation with Piezotechnology Inc, on the characterization of new piezoelectric materials, namely langatate, langanite, and langasite, and with bulk and surface acoustic wave devices. Mauricio was a Professor in the Department of Electronic Engineering, Universidade de São Paulo until he joined the Department of Electrical and Computer Engineering at the University of Maine in 2001, where he presently holds the position of Associate Professor.

Dr. Pereira da Cunha is a member of the IEEE, Sigma Xi, and of the Brazilian Microwave Society (SBMO). He was elected to serve on the SBMO Administrative Committee from 1996 to 1999. He is a reviewer and an associate editor for the *IEEE Transactions on Ultrasonics, Ferroelectrics, and Frequency Control*, and he has been a member of the IEEE International Ultrasonics Symposium Technical Program Committee since 1997. He served on the UFFC Society Administrative Committee from 2002 to 2004, served as Technical Program Committee Chair for the IEEE 2007 Ultrasonics Symposium, in New York, NY, as Vice-Chair for Ultrasonics from 2006 to 2008, and as Vice-President for Ultrasonics during 2009 and 2010. He has more than 140 journal and conference papers and presentations in the area of microwave acoustic propagation, acoustic wave material properties, bulk and surface acoustic wave modeling and devices, and sensors.